International Forum on Aeroelasticity and Structural Dynamics
IFASD 2017
25-28 June 2017, Como - Italy

STUDY ON ADAPTIVE WING STRUCTURE FOR COMPROMISING STRUCTURAL STRENGTH AND AERODYNAMIC PERFORMANCE

TAMAYAMA Masato[1], FUJII Kanata[2], YOKOZEKI Tomohiro[2], and ARIZONO Hitoshi[2]

[1] Aeronautical Technology Directorate
Japan Aerospace Exploration Agency, JAXA
tamayama.masato@jaxa.jp

[2] Department of Aeronautics and Astronautics
The University of Tokyo

Keywords: adaptive wing, aeroelasticity, structural analysis.

Abstract: The relation between aerodynamic induced drag and bending moment for the adaptive wing is studied analytically. Four flaps are attached to each of the wing leading- and trailing-edges, and they are applied with independent deflection angles. Totally 3,436 combinations of flap deflection angles are analyzed for the cruise condition of Mach number 0.78. The Static aeroelasticity analysis of MSC/NASTRAN using linear aerodynamics are conducted to acquire the aerodynamic pressures acting on the wing. The aerodynamic induced drag and the bending moment are derived from these pressure distributions. The analyzed results indicate that there is the Pareto Optimization Curve between the aerodynamic induced drag and the wing root bending moment. It is pointed out that the combinations of flap deflection angles on the Pareto Optimization Curve are effective if the aerodynamic performance is required adding to the structural healthiness.

1 INTRODUCTION

The demand for fuel-efficient aircraft has been expanding to seek for economic and environmental benefit. For this purpose, carbon fiber reinforced plastics(CFRPs) and high Aspect Ratio(AR) wing designs have been introduced into newly developed airplanes. However, the high aspect ratio wings easily lead to a lack of structural strength. This worry is enlarged during the gust encountering and the high maneuver load flights. The easiest prescription for these occasions is to increase the wing stiffness, though it usually lets aircraft heavier. To compromise the wing strength and the aerodynamic performance, an adaptive wing structure is considered in this study.

The adaptive wing is able to control the aerodynamic forces loaded on the wing during flights: the typical example of this wing is the one having a variable camber flap mechanism at its leading- and trailing-edges. The flaps are distributed along the span-wise direction. Aircraft wings are generally designed to make its flight performance optimized for a specific flight condition or sub-optimized for a specific flight interval during its cruise phase. Contrary to this conventional design, the adaptive wing can control the aerodynamic force distribution to be suitable for the aircraft condition at every moment during the flight.

The application of adaptive wings has been studied by many researchers. Rodriguez et al. conducted aeroelasticity analysis for a wing of Generic Transport Model (GTM) aircraft with the adaptive wing which is controlled by the Variable Camber Continuous Trailing Edge Flap(VCCTEF) system. And they showed the wave drag reduction by the VCCTEF. [1] Lebofsky et al. showed the reduction of maximum bending moment of Truss-Braced Wing(TBW) by the VCCTEF. [2] Tamayama et al. applied an adaptive wing to High Altitude Long Endurance aerial vehicle(HALE) having the wing AR of about 20, and showed a significant reduction of the wing root bending moment. [3]

In this study, the Objective Stress Reduction(OSR) by an adaptive wing is proposed. The focal point of the OSR is not only the reduction of wing root bending moment, but also the reduction of an extent of high stress area. In future, CFRPs will be used in aircraft's parts widely expecting weight reduction. In that situation, one of the major concerns is the significant deterioration in strength due to damages. [4] Structural Health Monitoring(SHM) technologies have been researched to probe damages. [5] In addition, strain measurement methods to be utilized to SHMs have also been developed. [6,7] With these technologies, it is possible to detect damages, to inverse estimation of load distribution, and to construct OSR control for reducing the stress of the damaged area by changing aerodynamic load distributions.

The performance of OSR is presented in this paper by static aeroelasticity analysis for the adaptive wing model, which has four deflectable flaps at each of the leading- and trailing-edges. The result of analysis obviously shows the trade-off characteristic between the aerodynamic performance and the structural benefit.

2 WING MODEL

The wing model used in this study is based on the JAXA Technology Reference Aircraft (TRA) 2012A model, which is the 120-passenger transport aircraft model designed to include the features of present conventional aircraft. [8] The specification of JAXA TRA2012A is shown in Table 1. By using these values, the semi-span wing model is constructed as shown in Table 2 and Figure 1. The chord length and the wing thickness vary linearly in the span-wise direction. The wing section is the 'NASA/Langley Whitcomb Integral Supercritical Airfoil.' [9]. There are 4 flaps at each of the wing leading- and trailing-edges, which equally have a span-wise length of 3,800 mm. Those flaps are named as the ' LEF *i* ' for the leading-edge ones and the ' TEF *i* ' for the trailing-edge ones: ' *i* ' is the flap identification number counting from the most inboard one.

Cruise Mach Number	0.78
Wing Area	1.224×10^8 mm^2
Aspect Ratio of Wing	9.5
Fuselage Diameter	3,700 mm
Coefficient of Lift at Cruise	0.5194
Cruise Altitude	35,000 ft. (10,668m / same as A319)

Table 1: Specification of JAXA TRA2012A.

In aeroelasticity analysis, structural and aerodynamic models are required. The former model is shown in Figure 2. It is composed of spars, ribs and skins. The material is ultra-duralumin. The spars are placed at 15% and 60% chord lines. Each flap section has 7 ribs. The wing is divided into 15 and 96 shell elements in the chord- and span-wise directions, respectively.

Swept-back angle at 25% chord line	0 °
Dihedral angle	0 °
Root chord length / wing thickness	5,102 mm / 559 mm
Tip chord length / wing thickness	1,656 mm / 181 mm
Wing taper ratio	0.3
Semi-span length	15,200 mm
Flap length in span-wise direction	3,800 mm / each

Table 2: Specification of present wing model.

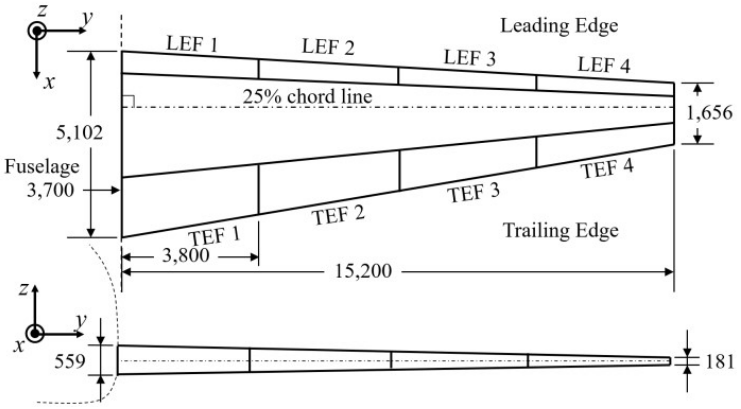

Figure 1: Two-view drawing of wing model [mm].

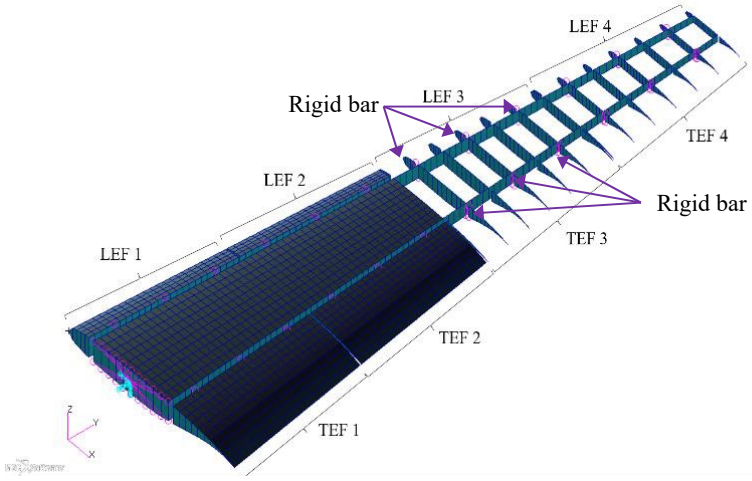

Figure 2: Structural model (the flap sections of i=3 and 4 are skeleton for better visibility).

The thicknesses of each member at the wing root and tip are shown in Table 3. These values vary linearly in the span-wise direction. The flaps are attached to the wing box with rigid bar elements: their locations are placed at the 2nd, 4th and 6th ribs of each flap as shown in Figure 2. The wing box root is set as a fixed boundary condition.

Element		Root [mm]	Tip [mm]
Spar		4.0	2.0
Rib		4.0	2.0
Skin	Wing Box	13.5	4.0
	Flap	4.0	2.0

Table 3: Thickness of Structural Elements

The aerodynamic model is shown in Figure 3. Aerodynamics is calculated by the lifting surface theory of MSC/NASTRAN. The model is a plate, and divided into 20 and 40 elements in the chord- and span-wise directions, respectively. The airfoil's camber and flap deflections are given with a downwash acting on each panel. The inputs into the calculations are the Mach number, dynamic pressure, angle of attack, and downwash distribution: the output is the aerodynamic force acting on each aerodynamic panel. By summing the aerodynamic force acting on each panel, the lift and bending moment distributions are calculated.

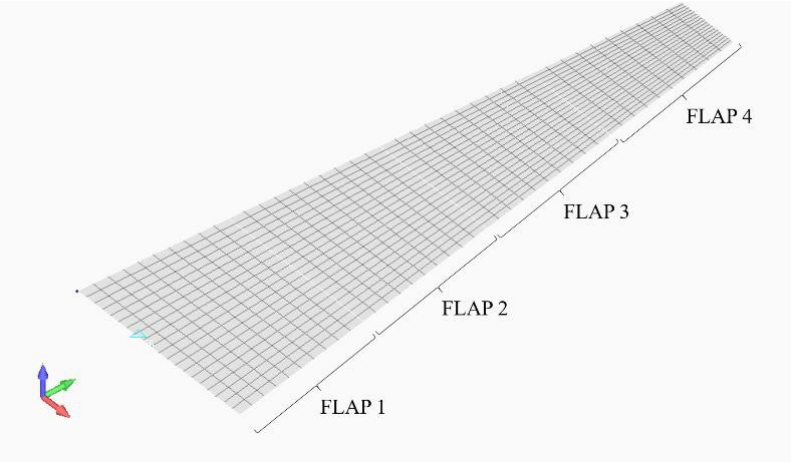

Figure 3: Aerodynamic model.

3 ANALYSIS

The cruise flight condition is considered in this paper. Its Mach number and altitude are 0.78 and 35,000 ft., respectively, referring to the JAXA TRA2012A. The wing configuration with all flaps deflecting by 0° is taken as the 'Base Flight Condition.' To sustain the cruising lift for the Base Flight Condition, the wing angle of attack is set to 1.1°: its specifications calculated by MSC/NASTRAN are presented in Table 4.

Total Lift, $L_{total,0}$ [N]		2.721×10^5
Maximum Bending Moment, $M_{max,0}$ [Nmm]		1.665×10^9
Maximum von-Mises Stress [MPa]	Spar	123.3
	Rib	126.7
	Skin	57.10

Table 4: Determination of Base Flight Condition.

In this paper, only the bending moment is discussed: the reason why is an influence of bending moment on wing stress is crucial for a high AR wing. Buckling possibility is not considered in this study, because the structural model is too primitive to do realistic considerations on buckling occurrences.

3.1 Determination of bending moment and aerodynamic induced drag

The parameters of this study are flap deflection angles, which vector expression is $\{\delta\}$ as shown in Eq. (1).

$$\{\delta\}^T = \{\delta_{LEF1}, \cdots, \delta_{LEF4}, \delta_{TEF1}, \cdots, \delta_{TEF4}\} \tag{1}$$

Figure 4: Definition of flap angle sign(i=1~4).

Figure 4 shows the definition of flap angle sign. Nose-up is positive for the LEFs and nose-down is positive for the TEFs. Two constraints are introduced in this study. One is the limit of flap deflections as follows:

$$-10° \le \delta_{\mathrm{LEFi}}, \delta_{\mathrm{TEFi}} \le +10° \tag{2}$$

In this study, only the linear aerodynamics is considered, and large flap deflections are inappropriate. The second constraint is applied to the variation in the total lift force $L_{total}(\delta)$ from $L_{total,0}=L_{total}(0)$, which corresponds to the total lift force of the Base Flight Condition. In order to maintain the cruise flight condition, the deviation of $L_{total}(\delta)$ from $L_{total,0}$ is set to 1 %:

$$\left| \frac{L_{total}(\delta) - L_{total,0}}{L_{total,0}} \right| \le 0.01 \tag{3}$$

The bending moment distribution $M(y)$ is calculated from the span-wise lift distribution $L'(y)$ as follows:

$$M(y) = \int_y^{b/2} L'(\eta)(\eta - y) d\eta \tag{4}$$

Here, y and η are the span-wise locations, and b is the full span length.

The aerodynamic induced drag C_{Di} is influenced by $L'(y)$ referring to lifting line theory. [10] Consider $L'(y)$ can be written as a sum of sine functions as follows:

$$L'(\theta) = 2b\rho_\infty V_\infty^2 \sum_{n=1}^{N} A_n \sin n\theta, \quad y = -\frac{b}{2}\cos\theta \tag{5}$$

Here, ρ_∞ is air density at cruising altitude and V_∞ is cruising velocity. With the series of A_n, C_{Di} can be written as follows:

$$C_{Di} = \pi AR\, A_1^2 \left(1 + \sum_{n=2}^{N} n A_n^2 \right) \tag{6}$$

3.2 Sets of flap deflection angles

To avoid analyzing enormous combinations of flap deflection angles, the following procedures are introduced. At first, approximate $L_{total}(\delta)$ as a quadratic polynomial of $\{\delta\}$ elements. This function is approximated from 100 analyzed results: these analyzed cases are determined by Central Composite Design, which is often used in Response Surface Method. The resultant function of $L_{total}(\delta)$ is utilized to select the combination of flap deflection angles to satisfy Eq.(3): this process will be conducted in the next step.

The next step is to calculate aerodynamic force distributions for the combinations of flap deflection angles. The deflection angles to be explored are shown in Table 5. To reduce the total number of cases to be analyzed, only some discrete values of deflection angles are selected in this study. The number of variations of LEF deflection angles are less than the TEF's ones, because the LEFs are less effective in altering lift distributions than the TEFs. For reducing bending moment, the common sense is to reduce the lift force acting on wing outboard area. According to this sense, the selected deflection angles of the outboard TEFs are biased toward minus sign, which has a tendency to generate negative lift. On the contrary, the selected values for the inboard TEFs are biased toward plus sign. Even if these efforts are applied to this study to reduce the case numbers, there are still totally 1,500,625 cases to be analyzed. Then, the quadratic polynomial function of $L_{total}(\delta)$ approximated in the previous process is utilized to determine whether the combination of flap deflection angles satisfies Eq.(3). Finally, the number of cases to be analyzed is reduced to 3,436.

Flap	Deflection angle [°]
LEF1,LEF2,LEF3,LEF4	-10, -5, 0, +5, +10
TEF1,TEF2	-2, 0, +2, +4, +6, +8, +10
TEF3,TEF4	-10, -8, -6, -4, -2, 0, +2

Table 5: Flap deflection angles to be explored.

4 RESULTS AND DISCUSSIONS

Figure 5 shows the results $\{C_{Di}, M_r\}$ of the analyzed cases: M_r is the wing root bending moment and equal to $M(0)$. Although the results are scattered in the figure, there exists an envelope curve. This is the Pareto Optimization Curve(POC). Consider the case corresponding to the point E. The common sense for a good wing is to have less aerodynamic drag and structural stress. If the C_{Di} is fixed, the performance of point G is better than that of point E. And, if the M_r is fixed, the performance of point F is better than that of point E. That is why the curve shown in Figure 5 is the POC. To consider the trade-off between the aerodynamic induced drag and structural stress, the cases on the POC should be chosen.

There is the case having the minimum C_{Di} in Figure 5. and call this case as the 'Case A.' The corresponding lift distribution $L'(y)$ is shown in Figure 6 with diamond marks. The results of Base Flight Condition are also shown in Figures 5 and 6: the lift distribution of Base Flight Condition is drawn as a curve. In Figure 6, the elliptic lift distribution is shown with triangle marks, which is known as the lift distribution having minimum induced drag. The lift distribution of Base Flight Condition slightly departs from the elliptic one. The wing geometry influences this discrepancy: the wing planform is linearly tapered in the span-wise direction in this study. For the Case A, the lift distribution agrees well with the elliptic one, and, therefore, it marks the minimum induced drag in Figure 5.

On the POC, the minimum M_r appears at the right edge, and call this case as the 'Case D.' In Figure 5, the bird's-eye views of flap deflections are also inserted. For the Case D, the most inboard trailing edge flap, TEF_1, deflects by the maximum deflection angle, and the outboard trailing edge flaps, TEF_3 and TEF_4, deflect by the minimum deflection angle. Caused by these flap deflections, the resultant lift distribution is apart from the elliptic distribution as shown in Figure 6. The $M(y)$ distributions shown in Figure 7 reflect the lift distributions. The $M(y)$ distribution of Case D is much less than that of Case A. The quantitative information is presented in Table 6.

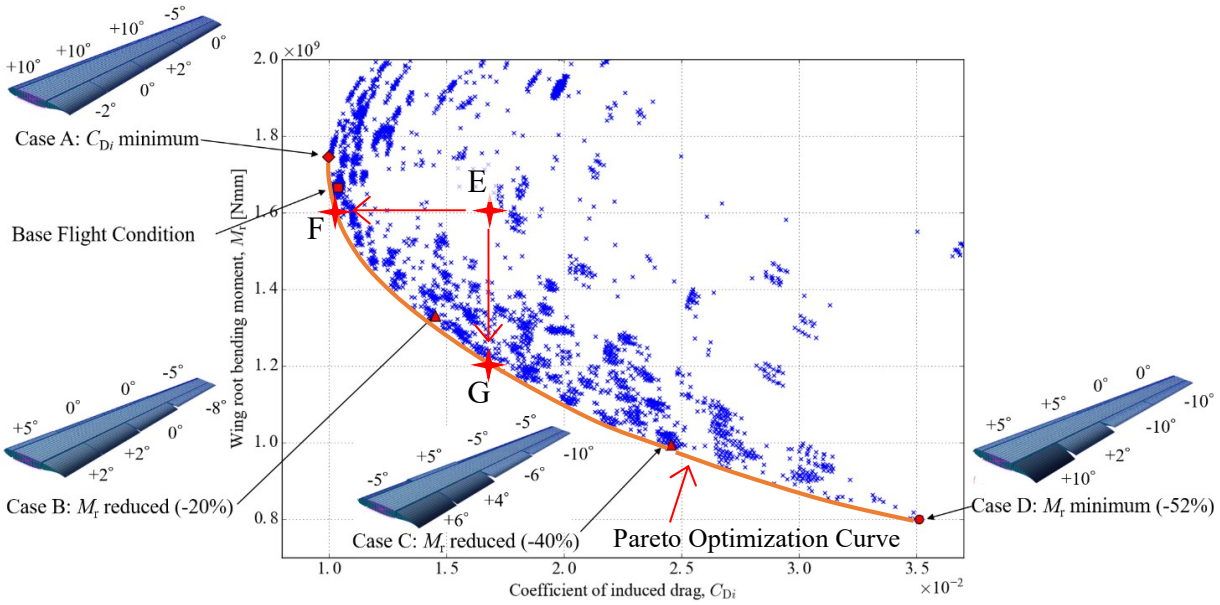

Figure 5: Wing root bending moment vs. coefficient of induced drag.

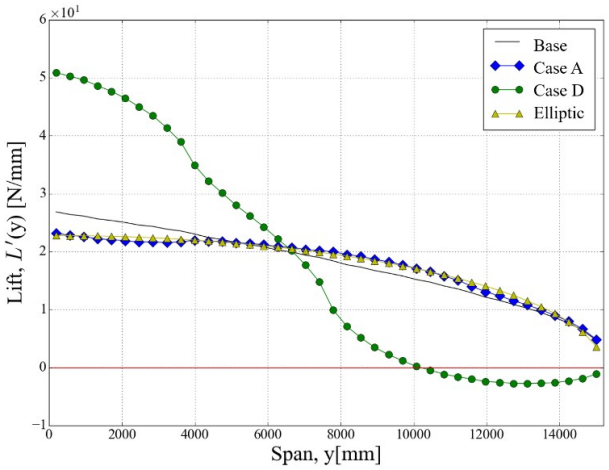

Figure 6: Span-wise lift distributions.

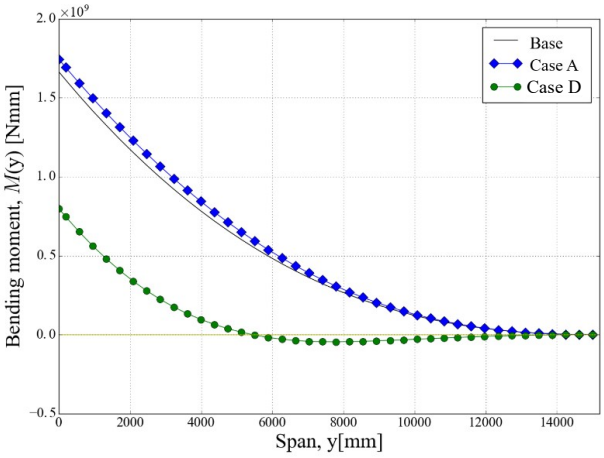

Figure 7: Bending moment distributions.

	Wing root bending moment M_r [$\times 10^9$ Nmm]	Coefficient of induced drag C_{Di} [$\times 10^{-2}$]
Base flight condition	1.665 (±0.00 %)	1.037 (±0.00 %)
Case A	1.745 (+4.8 %)	0.9974 (-3.82 %)
Case D	0.7996 (-52.0 %)	3.511 (+239 %)

Table 6: Wing root bending moment and coefficient of induced drag.

The results of Cases A and D are the edges of the POC in this study. Also, consider the cases between these edges: the Cases B and C which correspond to 20 and 40 % M_r reductions from that of Base Flight Condition, respectively. Figure 8 is the lift distributions and Figure 9 is the $M(y)$ distributions for the Cases B, C and D. If the wing structure get suffered from a damage, the stress in the structure should be kept under a certain stress level, which must be smaller than that of original structure to keep the structural healthiness. Although Figure 9 is the distribution of M(y) and does not give us stress information, let's consider the reevaluated strength criterion level as the Line H in Figure 9. If the wing receives a damage at the location P in Figure 9, all of Cases B, C and D can work. Therefore, the Case B is the best combination of flap deflection angles to seek better aerodynamic performance adding to the structural healthiness. On the other hand, if the damage location is Q in Figure 9, only the Case D can work.

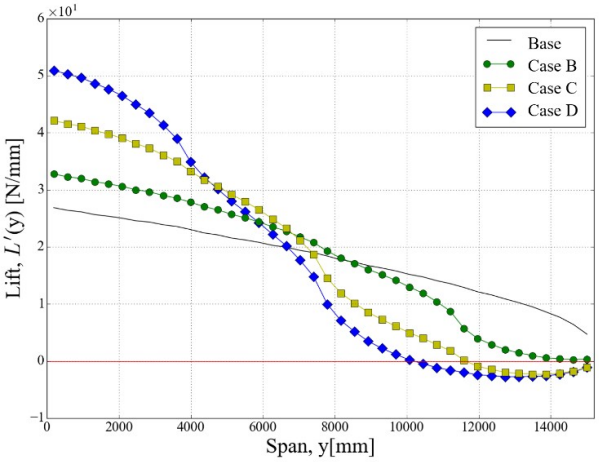

Figure 8: Span-wise lift distributions of Cases B, C and D.

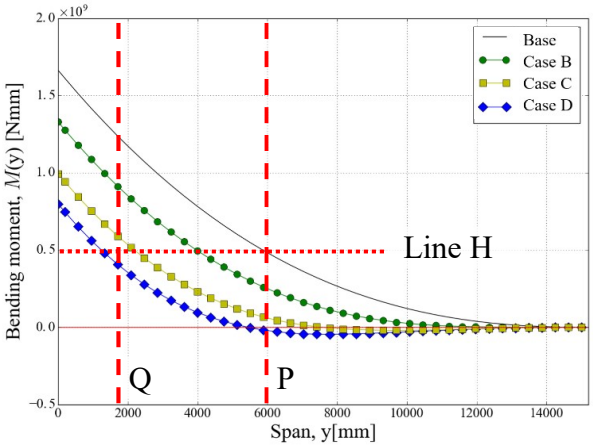

Figure 9: Bending moment and torsional moment distributions of Cases B, C and D.

Are the combinations of flap deflection angles other than those on the POC insignificant? Although Figure 5 shows only the results of cruise condition, similar figures can be made for other flight conditions whose load factor is greater than 1. For those flight conditions, the Maneuver Load Alleviation(MLA) is important to enhance the fatigue performance. If only the combinations of flap deflection angles on the POC are used for the MLA, the highest stress is generated at the same area every time. If the combinations other than those on the POC are introduced into the MLA, the highest stress area varies in the wing structure depending on the combination of flap deflection angles and it might enhance the fatigue performance.

5 CONCLUSIONS

The characteristics of an adaptive wing is studied analytically in this research. The analytical wing model is constructed referring to the JAXA's TRA2012A model. Four flaps are mounted on each of the wing leading- and trailing-edges, and they are applied with independent deflection angles. By applying constraints to the analysis and approximating the lift distributions with a quadratic polynomial function of $\{\delta\}$, the case number in the exploring field is reduced from 1,500,625 to 3,436. The Static aeroelasticity analysis of MSC/NASTRAN using lifting surface theory are conducted to acquire the aerodynamic pressures acting on the wing at the cruise Mach number of 0.78. The aerodynamic induced drag and the bending moment are derived from these pressure distributions. From these results, the conclusions are given as follows:

- There is the combination of flap deflection angles having better aerodynamic performance than the Base Flight Condition. This is caused by the fact that the planform of present wing model is linearly tapered in the span-wise direction and does not generate an elliptic lift distribution.
- The analyzed results indicate that there is a Pareto Optimization Curve between the aerodynamic induced drag and the wing root bending moment.
- The combinations of flap deflection angles on the Pareto Optimization Curve are effective if aerodynamic performance is required adding to structural healthiness.
- If the combination of flap deflection angles on the Pareto Optimization Curve is used anytime, the highest stress is fixed at one area. The combinations of flap deflection angles other than those on the Pareto Optimization Curve might be useful to enhance the fatigue performance by varying the highest stress area.

The required lift is generated only by deflecting flaps in this research, but it is not realistic in actual flights. To fit the lift generation to actual flights, airplane pitch control is also introduced in our present progressive research.

6 ACKNOWLEDGEMENT

This study was partially conducted under the financial support of Grant-in-Aid for Scientific Research (No.15K06598) by Japan Society for the Promotion of Science.

7 REFERENCES

[1] Rodriguez, D. L., Aftosmis, M. J., Nemec, M. and Anderson, G. R. (2015). Optimized Off-Design Performance of Flexible Wings with Continuous Trailing-Edge Flaps. AIAA Paper 2015-1409.

[2] Lebofsky, S., Ting, E., Nguyen, N. and Trinh, K. (2015). Optimization for Load Alleviation of Truss-Braced Wing Aircraft with Variable Camber Continuous Trailing Edge Flap. AIAA Paper 2015-2723.
[3] Tamayama, M., Fujii, K., Arizono, H. and Yokozeki, T. (2015). Bending Moment Reduction of a High Aspect Ratio Wing. 25th International Conference on Adaptive Structures and Technologies, ICAST2015-#32, Kobe, Japan.
[4] Rivallant, S., Bouvet, C., Abdallah, E.A., Broll, B. and Barrau, JJ.(2014). Experimental analysis of CFRP laminates subjected to Compression After Impact: the role of impact-induced cracks in failure. Composite Structures, Elsevier, 2014, vol. 111, pp.147-157.
[5] Okabe, Y., Fujibayashi, K., Shimazaki, M. and Soejima, H. (2011). Damage Detection in Aircraft Composite Materials Using a Built-in Broadband Ultrasonic Propagation System. Journal of System Design and Dynamics, Vol. 5, No. 5, Special Issue of Motion and Vibration Control 2010, pp.966-981.
[6] Takeda, S., Aoki, Y. and Nagao, Y. (2012). Damage Monitoring of CFRP Stiffened Panels under Compressive Load Using FBG Sensors. Composite Structures, 94, pp. 813-819.
[7] Wada, D., Igawa, H. and Kasai, T. (2016). Vibration monitoring of a helicopter blade model using the optical fiber distributed strain sensing technique. Applied Optics, Vol. 55, Issue 25, pp.6953-6959.
[8] Kwak, D., Tamayama, M., Nomura, T. and Arizono, H. (2015). Preliminary Studies on the Lift Distribution and Aspect Ratio of Subsonic Aircraft Wing for Fuel Consumption Reduction. Proceedings of 53rd JSASS Aircraft Symposium, Paper No. 3A12 (in Japanese).
[9] UIUC Airfoil Coordinate Database (cited 1 August 2016). http://m-selig.ae.illinois.edu/ads/coord_database.html.
[10] Anderson Jr., J. D.(1991). Fundamentals of Aerodynamics Second Edition. McGraw-Hill, New York, pp. 335-338.

COPYRIGHT STATEMENT